Orbital Physics in Transition-Metal Oxides

Y. Tokura, *et al.*

Science **288**, 462 (2000);
DOI: 10.1126/science.288.5465.462

REVIEW

Orbital Physics in Transition-Metal Oxides

Y. Tokura[1,2] and N. Nagaosa[1]

An electron in a solid, that is, bound to or nearly localized on the specific atomic site, has three attributes: charge, spin, and orbital. The orbital represents the shape of the electron cloud in solid. In transition-metal oxides with anisotropic-shaped d-orbital electrons, the Coulomb interaction between the electrons (strong electron correlation effect) is of importance for understanding their metal-insulator transitions and properties such as high-temperature superconductivity and colossal magnetoresistance. The orbital degree of freedom occasionally plays an important role in these phenomena, and its correlation and/or order-disorder transition causes a variety of phenomena through strong coupling with charge, spin, and lattice dynamics. An overview is given here on this "orbital physics," which will be a key concept for the science and technology of correlated electrons.

The quantum mechanical wave function of an electron takes various shapes when bound to an atomic nucleus by Coulomb force. Consider a transition-metal atom in a crystal with perovskite structure. It is surrounded by six oxygen ions, O^{2-}, which give rise to the crystal field potential and hinder the free rotation of the electrons and quenches the orbital angular momentum by introducing the crystal field splitting of the d orbitals. Wave functions pointing toward O^{2-} ions have higher energy in comparison with those pointing between them. The former wave functions, $d_{x^2-y^2}$ and $d_{3z^2-r^2}$, are called e_g orbitals, whereas the latter, d_{xy}, d_{yz}, and d_{zx}, are called t_{2g} orbitals (Fig. 1).

When electrons are put into these wave functions, the ground state is determined by the semiempirical Hund's rule. As an example, consider $LaMnO_3$, where Mn^{3+} has a d^4 configuration, i.e., four electrons in d orbitals. Because of Hund's rule, all of the spins are aligned parallel, that is, $S = 2$, and three spins are put to t_{2g} orbitals and one spin occupies one of the e_g orbitals.

The relativistic correction gives rise to the so-called spin-orbit interaction $H_{\text{spin-orbit}} = \lambda \vec{L} \cdot \vec{S}$, where $\vec{L}$ is the orbital angular momentum and $\vec{S}$ is the spin angular momentum. This interaction plays an important role in some cases, especially for t_{2g} electrons. However, the coupling between spin and orbital degrees of freedom described below is not due to this relativistic spin-orbit coupling.

Up to now, we have considered only one transition-metal ion. However, in solids, there are periodic arrays of ions. There are two important aspects caused by this: one is the magnetic interactions, i.e., exchange interactions, between the spins and the other is the possible band formation and metallic conduction of the electrons. Before explaining these two, let us introduce the Mott insulating state. Band theory predicts an insulating state when all bands are fully occupied or empty, whereas a metallic state occurs under different conditions. However, it is possible that the system is insulating because of the Coulomb interaction when the electron number is an integer per atom, even if the band theory without the period doubling predicts a metallic state. This occurs when the kinetic energy gain is smaller and blocked by the strong Coulomb repulsion energy U, and the electron cannot hop to the other atom. This insulator is called a Mott insulator. The most important difference from the usual band insulator is that the internal degrees of freedom, spin and orbital, still survive in the Mott insulator. $LaMnO_3$ is a Mott insulator with spin $S = 2$ and the orbital degrees of freedom. The spin $S = 2$ can be represented by the t_{2g} spin 3/2 strongly coupled to the e_g spin 1/2 with ferromagnetic J_H (Hund's coupling). The two possible choices of the orbitals are represented by the pseudospin $\vec{T}$, whose z component $T_z = 1/2$ when $d_{x^2-y^2}$ is occupied and $T_z = -1/2$ when $d_{3z^2-r^2}$ is occupied. Three components of this pseudospin satisfy the similar commutation relation with those of the spin operator, i.e., $[T_\alpha, T_\beta] = i\varepsilon_{\alpha\beta\gamma}T_\gamma$.

There is an interaction between the spin and pseudospin, of $\vec{S}$ and $\vec{T}$, between different ions. This exchange interaction is represented by the following generalized Heisenberg Hamiltonian (*1*):

$$H = \sum_{ij} [J_{ij}(\vec{T}_i, \vec{T}_j)\vec{S}_i \cdot \vec{S}_j + K_{ij}(\vec{T}_i, \vec{T}_j)] \quad (1)$$

The exchange interactions J_{ij} and K_{ij} originate from the quantum mechanical process with intermediate virtual states (*2, 3*). The rotational symmetry in the spin space leads to the inner product form of the interaction. When more than two orbitals are involved, a variety of situations can be realized, and this quantum mechanical process depends on the orbitals (*4, 5*). In this way, the spin $\vec{S}$ and the orbital pseudospin $\vec{T}$ are coupled. In more general cases, the transfer integral t_{ij} depends on the direction of the bond ij and also on the pair of the two orbitals a, $b = (x^2 - y^2)$ or $(3z^2 - r^2)$. This gives rise to the anisotropy of the Hamiltonian in the pseudospin space as well as in the real space. For example, the transfer integral between the two neighboring Mn atoms in the crystal lattice is determined by the overlaps of the d orbitals with the p orbital of the O atom between them. The overlap between the $d_{x^2-y^2}$ and p_z orbitals is zero because of the different symmetry with respect to the holding in the xy plane. Therefore, the electron in the $d_{x^2-y^2}$ orbital cannot hop along the z axis. This fact will be important later in our discussion.

One can consider the long-range ordered state of the orbital pseudospin $\vec{T}$ as well as the spin $\vec{S}$. In many respects, analogies can be drawn between $\vec{S}$ and $\vec{T}$ in spite of the anisotropy in $\vec{T}$ space. However, there is one more aspect that is special to $\vec{T}$—Jahn-Teller (JT) coupling (*6–8*). Because each orbital has different anisotropy of the wave function, it is coupled to the displacement of the O atoms surrounding the transition-metal ion. For example, when the two apical O atoms move toward the ion, the energy of $d_{3z^2-r^2}$ becomes higher than $d_{x^2-y^2}$ and the degeneracy is lifted. This is called the JT effect (*6*) and is represented by the following Hamiltonian for a single octahedron:

$$H_{JT} = -g(T_xQ_2 + T_zQ_3) \quad (2)$$

where (Q_2, Q_3) are the coordinates for the displacements of O atoms surrounding the transition-metal atom and g is the coupling constant. When the crystal is considered, (Q_2, Q_3) should be generalized to (Q_{i2}, Q_{i3}) (i, the site index), which is represented as the sum of the phonon coordinates and the uniform component (u_2, u_3). Here, (u_2, u_3) describes the crystal distortion as a whole. When the long-range orbital order exists, i.e., $\langle T_{ix} \rangle \neq 0$ and/or $\langle T_{iz} \rangle \neq 0$, the JT distortion is always present.

Up to now, we have discussed the Mott insulating state. Let us now consider the doped carriers into a Mott insulator. High-transition-temperature superconductor cuprates, e.g., $La_{2-x}Sr_xCuO_4$, offer the most dramatic example of this carrier doping. However, the two-dimensional (2D) nature of the lattice, as well as the larger coherent

[1]Department of Applied Physics, University of Tokyo, Bunkyo-ku, Tokyo 113-8656, Japan. [2]Joint Research Center for Atom Technology, Tsukuba 305-0046, Japan.

(F) JT distortion for the Cu^{2+}–O sheet, gives a large energy splitting between $d_{3z^2-r^2}$ and $d_{x^2-y^2}$ orbitals, and only $d_{x^2-y^2}$ is relevant (the orbital degrees of freedom are quenched). In the case of $La_{1-x}Sr_xMnO_3$, Mn^{4+} or holes with concentration x are doped, and still, the orbital degrees of freedom are active. The most important and fundamental interaction in the doped case is the double-exchange interaction (*9, 10*). e_g electrons are forced to be parallel to the localized t_{2g} spins by the strong J_H. When an e_g electron hops from atom i to j, at each atom the spin wave function $|\chi\rangle$ of the e_g electron is projected to $|\chi_i\rangle$ and $|\chi_j\rangle$ corresponding to the spin direction of each t_{2g} spin. Therefore, the effective transfer integral is given by $t_{ij} = t\,\langle\chi_i|\chi_j\rangle$, which depends on the relative direction of the two spins; $|t_{ij}| = t|\langle\chi_i|\chi_j\rangle| = t\cos(\theta_{ij}/2)$ (θ_{ij}, the angle between the two spins) is maximum for parallel spins and is zero for antiparallel spins. Therefore, the kinetic energy gain of the doped holes is maximized for parallel spins, which gives the ferromagnetic interaction between the spins. This is called double-exchange interaction.

Manganese Oxides as a Prototype

An active role of orbital degree of freedom in the lattice and electronic response can be most typically seen in manganese oxide compounds with perovskite structure. In this class of compounds, colossal magnetoresistance (CMR), i.e., a very large decrease of resistance, is observed upon the application of an external magnetic field and has attracted a lot of interest (*11*). The CMR phenomenon itself is, as argued in the following, most relevant to the orbital ordering and correlation.

The orbital ordering gives rise to the anisotropy of the electron-transfer interaction. This favors or disfavors the double-exchange interaction and the superexchange (ferromagnetic or antiferromagnetic) interaction in an orbital direction–dependent manner and hence gives a complex spin-orbital coupled state. One typical example is the case of $LaMnO_3$ with no double-exchange carriers, in which the in-plane (*ab* plane) alternate ordering of $(3x^2 - r^2)/(3y^2 - r^2)$ orbitals causes the in-plane ferromagnetic spin coupling. This A-type antiferromagnetic (AF) state is the manifestation of the anisotropic superexchange interactions, that is, ferromagnetic within the plane and AF between the plane, due to the orbital ordering.

The importance of the orbital and lattice degrees of freedom has long been recognized theoretically (*12*). The spin and orbital order has been studied for the realistic model Hamiltonian Eq. 1 in the mean field approximation. As for the e_g electrons in 3D perovskite structure, the A-type AF state is obtained with alternating $(z^2 - x^2)/(y^2 - z^2)$ orbitals within the plane. In addition to this superexchange interaction, the Jahn-Teller interaction (JTI) also contributes to determining the orbital ordering. When JTI prefers the planar orbitals, such as $(z^2 - x^2)$ and $(y^2 - z^2)$, it does not contradict with the above orbital ordering; however, JTI could also prefer the rod-type orbitals, such as $(3z^2 - r^2)$. In the former case and/or when JTI is weak, the A-type AF state with alternating $(z^2 - x^2)/(y^2 - z^2)$ orbitals should be realized as observed in $KCuF_3$ (*1*). The A-type AF state with alternating $(3x^2 - r^2)/(3y^2 - r^2)$ in $LaMnO_3$, on the other hand, is attributed to the JT distortion (*13–15*).

In the hole-doped manganese oxides, in which the double-exchange interaction emerges with the strength being dependent on the doping level, various orbital-ordered and disordered states show up, accompanying the respective spin-ordering features (Fig. 2, top). Let us here take the case of $Nd_{1-x}Sr_xMnO_3$ under ambient pressure (*16–19*). With appreciable doping on the parent compound $NdMnO_3$, the orbital order melts into a quantum-disordered state, and the compound shows the ferromagnetic-metallic (F) state for $0.3 < x < 0.5$. When doped further, the kinetic energy of carriers decreases, and the compound shows the 2D metallic state with layered-type antiferromagnetic (A) state for $0.5 < x < 0.7$. Doping above $x = 0.7$ further alters the magnetic structure to the chain type (C). This rich phase diagram can be reproduced and understood theoretically in terms of the mean field approximation applied to the generalized Hubbard model (*20*). The A state is realized as the compromise between the AF superexchange interaction between the t_{2g} spins and the double-exchange interaction through the ferromagnetic (homogeneous) order of $(x^2 - y^2)$ orbital (*20*). In cubic perovskite, the electron transfer is almost prohibited along the c axis because of the $(x^2 - y^2)$ orbital order, which is also the origin for the interplane AF coupling. In fact, the charge dynamics in this A-type AF state is almost 2D (*18*).

The C-type AF state for $x > 0.7$ is accompanied by the $(3z^2 - r^2)$ orbital. This state is perhaps affected also by the charge ordering and shows an insulating feature (Fig. 2A). The large orbital polarization $\vec{T}$ is indispensable for this rich phase diagram. The shape of the wave function is well defined, and the anistropy appears only in this case, i.e., the dimensional control by the orbital occurs. Otherwise, it would become a boring phase diagram in which the ferromagnetic state dominates.

Instead of changing the carriers' kinetic energy with doping level, one can use the lattice strain as a biasing field on the orbital state through the JT channel; namely, the uniaxial strain with respect to the MnO_6 octahedron can serve as a pseudo magnetic field on the pseudospin $\vec{T}$. Figure 2B shows a schematic spin-orbital phase diagram in the moderately doped ($0.3 < x < 0.7$) manganese oxides on the plane of the uniaxial strain measured as the ratio of lattice parameter c/a (or almost equivalently the ratio of the apical to equatorial Mn–O bond length) and the doping x. The phase diagram was based on the local density functional calculation as well as the experimental results for the epitaxial single-crystalline films of $La_{1-x}Sr_xMnO_3$ with coherent lattice strain due to the lattice mismatching with the substrate (*21*). The entanglement of the doping and the strain causes the slanted phase boundaries for the F (orbital-disordered), A

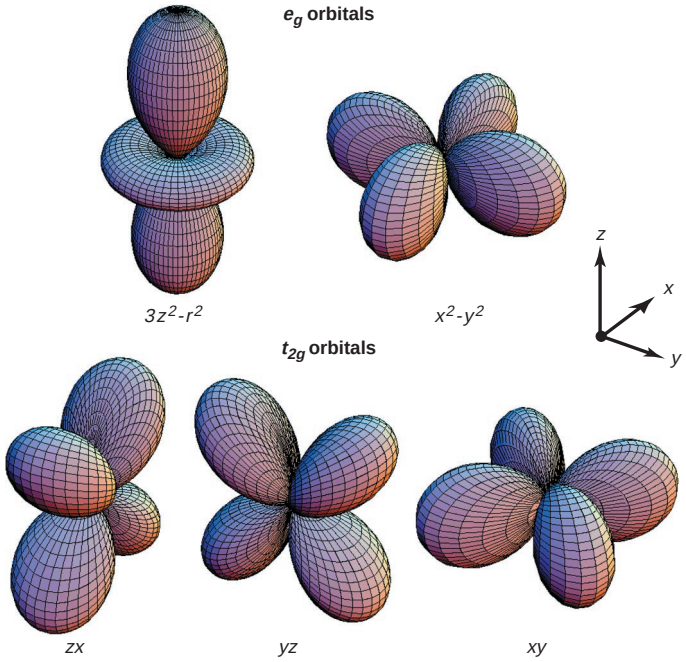

Fig. 1. Five d orbitals. In the cubic crystal field, this fivefold degeneracy is lifted to two e_g orbitals [$(x^2 - y^2)$ and $(3z^2 - r^2)$] and three t_{2g} orbitals [(xy), (yz), and (zx)].

[$(x^2 - y^2)$-ordered], and C [$(3x^2 - r^2)$-ordered] states. As a general trend, the decrease of hole doping enlarges the F region, whereas the increase (decrease) in the c/a ratio stabilizes the C (A) state as expected. In fact, thin films of $La_{1-x}Sr_xMnO_3$ ($x = 0.5$) epitaxially grown on three different perovskite substrates show the respective ground states (F, A, and C) and the similar transport properties to those shown in the case of $Nd_{1-x}Sr_xMnO_3$ (Fig. 2A).

The orbital ordering in the manganese oxides occasionally accompanies the concomitant charge ordering. The most prototypical case, namely the CE type shown in Fig. 3A, is realized at a doping level (x) of 0.5. In the pseudo cubic perovskite, the ab planes are coupled antiferromagnetically while keeping the same in-plane charge and orbital pattern (*22, 23*).

Theoretically, a band calculation with the local density approximation (LDA) combined with the on-site Coulomb interaction U has successfully reproduced the observed spin/charge/orbital–ordered state for $Pr_{1/2}Ca_{1/2}MnO_3$ (*24*). It is an important issue to identify the major driving force of the spin/charge/orbital ordering. The experimental observation in $Pr_{1/2}Ca_{1/2}MnO_3$ that the transition temperature of charge ordering is higher than that of antiferromagnetism suggests that the former is the driving force.

Once the zigzag chain structure is assumed for the orbital ordering, the electronic structure becomes 1D, and the sign alternation of the transfer integrals due to the antisymmetric combination of x^2 and y^2 in $(x^2 - y^2)$ plays some important roles (*25, 26*).

In the single-layered perovskite $La_{1-x}Sr_{1+x}MnO_4$ ($x = 0.5$), having the so-called K_2NiF_4 structure like La_2CuO_4, the same charge-orbital pattern (Fig. 3A) was confirmed by the resonant x-ray scattering method (*27*). In this compound, the charge and orbital ordering occurs concomitantly at the charge-ordering temperature $T_{CO} = 220$ K, and then the CE-type spin-ordering transition occurs at the AF temperature $T_N = 150$ K. At temperatures above T_{CO}, the average structure of the crystal is tetragonal, and hence, the optical property is isotropic in the lateral plane. Upon the orbital ordering, the crystal is deformed to orthorhombic, though hardly detected by conventional diffraction measurements. However, the anisotropic ordering of the orbital causes a fairly large in-plane anisotropy in the optical electronic transitions (*28*); hence, in the image with cross-polarized light, we can visualize the orbital-ordered domain (Fig. 3B). The orbital-disordered state above T_{CO} is optically isotropic in the plane, giving the extinction of cross-polarized reflection light, whereas we observe the globally bright image for the orbital-ordered state below T_{CO}, where the orthorhombic domain structure and domain walls (dark stripes) are clearly visible. (A periodic structure of the domains perhaps arises from the slight residual strain introduced during the process of the crystal growth.)

The CE-type orbital/charge–ordered state in the manganese oxides is generally amenable to an application of a magnetic field. The variation of the orbital/charge–ordered state is shown (Fig. 4) in the plane of magnetic field (H) and temperature (T) for the $x = 0.5$ perovskite manganites $R^{3+}_{0.5}A^{2+}_{0.5}MnO_3$, with various combinations of (R, A) (R and A are trivalent rare-earth and divalent alkaline-earth ions, respectively). The change in the average size of the (R, A) site controls a deviation of the Mn–O–Mn bond angle from 180° and hence controls the e_g electron-hopping interaction t through a change in Mn 3d and O 2p hybridization. With a decrease of the ionic radius, say from (Nd, Sr) to (Sm, Ca), the H-T region for the stable orbital/charge–ordered state is enlarged (Fig. 4). There are two types of orbital/charge/spin phase diagrams (*29*). In a relative wide-bandwidth system like $Nd_{0.5}Sr_{0.5}MnO_3$, the ferromagnetic ordering first occurs at the critical temperature T_c in the cooling process, and then at a lower temperature, the orbital, charge, and spin (AF) ordering occurs concomitantly at $T_{CO} = T_N$ (type I). The type I crystal undergoes the CE-type orbital/charge/spin–ordering transition only at the doping level very close to $x = 1/2$. In the smaller bandwidth system, say $Pr_{0.5}Ca_{0.5}MnO_3$, first the orbital and charge–ordered state appears concomitantly at $T_{CO} \cong 250$ K, and then the AF spin ordering takes place at a lower temperature T_N (type II). The ferromagnetic and metallic state is only realized under a magnetic field in this type. The crossover from type I to type II shows a complicated feature (*30*), but near such a multicritical point for the orders of orbital/charge and spin, a very large fluctuation and a critical field suppression seem to appear as typically seen in the CMR behavior.

The aforementioned orbital-charge correlation is a source of the high-resistance state above the ferromagnetic transition temperature T_C, which causes the CMR upon the

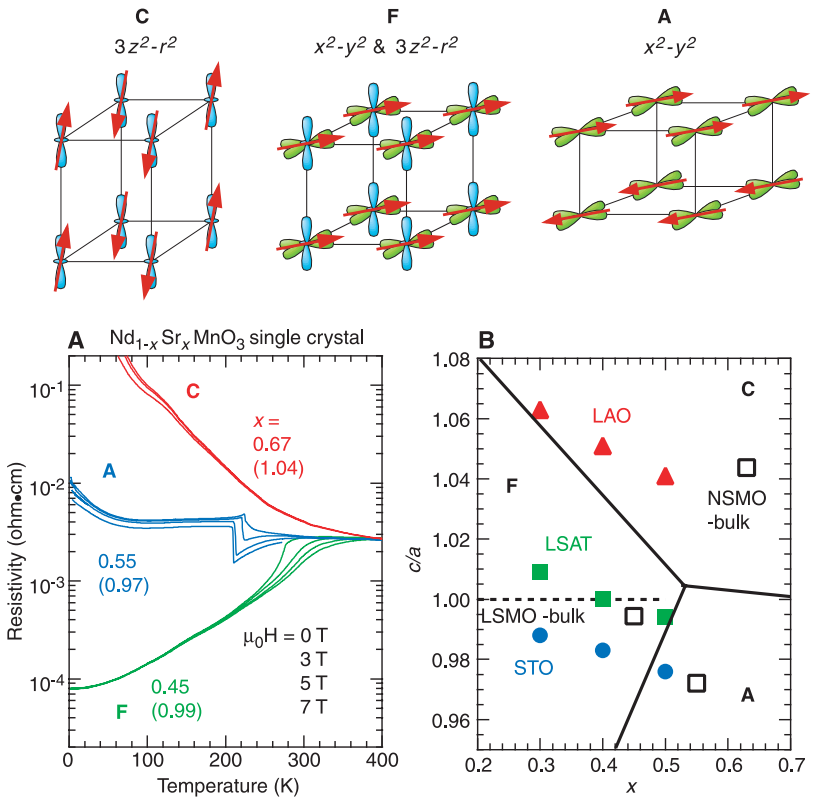

Fig. 2. Spin-orbital phase diagram in the perovskite manganese oxide. The top panel shows the orbital and spin order realized in the hole-doped manganese oxides. (**A**) Temperature dependence of resistivity in various magnetic fields $\mu_0 H$ for $Nd_{1-x}Sr_xMnO_3$ with the respective magnetic phases (F, A, and C). The numbers in parentheses represent the uniaxial lattice strain, c/a ratio, indicating the coupling of the magnetism to the orbital order as shown in the top panel. (**B**) The schematic phase diagram in the plane of lattice strain c/a and doping level x. The data labeled LAO, LSAT, and STO represent the results for the coherently strained epitaxial thin films of $La_{1-x}Sr_xMnO_3$ grown on the perovskite single-crystal substrates of $LaAlO_3$, $(La,Sr)(Al,Ta)O_3$, and $SrTiO_3$, respectively. LSMO-bulk and NSMO-bulk stand for the results for the bulk single crystals of $La_{1-x}Sr_xMnO_3$ and $Nd_{1-x}Sr_xMnO_3$, respectively.

application of a magnetic field. Even with no long-range orbital/charge ordering, the remnant of the short-range order can be clearly seen, for example, in diffuse x-ray scattering with the broad incommensurate peak (*31, 32*) and Raman phonon spectral anomaly (*33*). Figure 5 displays temperature variation of the CMR-related behavior for the $Sm_{1-x}Sr_x$-MnO_3 ($x = 0.45$) crystal on the verge of the aforementioned multicritical point between types I and II (*34, 35*). When the ferromagnetic double-exchange interaction competes with the charge/orbital ordering and extinguishes the long-range ordering, as in the present case, the superlattice x-ray peak, say (2, 1/2, 0) in the orthorhombic setting, arising from the CE-type orbital ordering (Fig. 3A), turns into incommensurate and diffuse scattering as exemplified in Fig. 5A. The diffuse scattering intensity measured at (2, 1.7, 0) increases with lowering temperature down to T_C and then suddenly drops below T_C (Fig. 5B). The temperature dependence compares well with that of resistivity change through T_C (Fig. 5C). All of the results, including the Raman phonon spectral anomaly, the AF spin correlation, and the in-plane expansion and *c*-axis compression of the lattice parameters above T_C (*35*), indicate that the orbital shows the dynamical and short-range (but directionally long-range) ordering above T_C that collapses immediately below T_C or in a magnetic field.

The orbital fluctuation in the doped manganese oxides may also be a cause for the highly incoherent charge dynamics, even in the ferromagnetic metallic state with full spin polarization (no spin fluctuation). According to the recent studies (*36–39*), the ferromagnetic ground state shows the very small spectral weight of the quasi-particle peak at the Fermi level in the photoemission spectrum as well as the minimal Drude weight in the optical conductivity spectrum. The Drude weight is, in fact, an order of magnitude smaller than expected from the results of the electronic specific heat coefficient (*39, 40*), indicating the least mass renormalization effect, and of the small Hall coefficient (*39*), indicating the metallic density of charge carriers.

Given the almost perfectly aligned spins, the only remaining degrees of freedom are the charge and orbital. Considering that the orbital polarization is large in the orbital-ordered state, it is reasonable that it remains so even in the ferromagnetic metallic state without the ordering. Therefore, it seems to be a promising scenario that these anomalous features come from the highly nonlocal scattering of the charge carrier due to the orbital correlation or short-range ordering such as $(x^2 - y^2)$ ordering (*41–43*). This situation is the orbital analog of the heavy fermions where the local spin polarization is induced, but its quantum fluctuation eventually leads to the singlet state caused by the Fermi degeneracy. Actually, the quantum mechanics of $\vec{T}$ shows low-dimensional dispersion similar to that discussed after Eq. 4, which enhances the quantum fluctuation and enables the quantum-disordered orbital state to remain stable down to zero temperature, i.e., orbital liquid state.

However, a variety of scenarios have been proposed so far for such an anomalously "bad metal" feature (*44–47*). The microscopic phase separation (*45–47*) is one of the most important candidates. In any case, further studies, both experimental and theoretical, are needed for this issue.

Other Materials and Theories

In the last section, we focused on manganese oxides, but the orbital physics are universal in transition-metal oxides. We review here some of the interesting features of orbital physics, both experimental and theoretical.

For the classic material V_2O_3, which has corundum structure, two electrons occupy t_{2g} orbitals. In the conventional view, the orbital ordering in the E_g state of the original t_{2g} manifold has been assigned to the origin of the specific spin order in the AF ground state (*48, 49*). An effective Hamiltonian for spin and orbital has been derived on the basis of this picture, and the magnetic properties were discussed. The important feature is that the magnetic exchange interaction depends on the orbital occupancy as represented in Eq. 1, i.e., even the sign could change. Therefore, it is possible that the magnetic correlation in the normal state can be very different from that in the ordered phase when the orbital order is accompanied by the magnetic transition, as observed experimentally (*50*). This strong interplay between the spin and orbital is thought to be the origin of a strong first-order phase transition. However, a recent article opposes this conventional picture and proposes the spin triplet ($S = 1$) formation at each V site (*51*).

A more transparent example is the case of perovskite type $RTiO_3$ and RVO_3 with $3d^1$ and $3d^2$ electron configuration, respectively, both retaining the orbital degree of freedom in the t_{2g} state. For example, a Mott insulator, $YTiO_3$, shows the ferromagnetic, not AF, ground state with ferromagnetic temperature T_C of ~30 K, a clear indication of some orbital order. According to the LDA calculation on $LaVO_3$ with the C-type or (π, π, 0) spin order and on YVO_3 with the G-type or (π, π, π) spin order, the orbital order is conjectured to take the G type and C type, respectively, converse to the spin order (*52*). A temperature-induced magnetization-reversal phenomenon observed in YVO_3 has been attributed to the combined effect of the single-spin anisotropy, Dzyaloshinsky-Moriya interaction, and the orbital transition (*53*). The actual orbital order pattern in these t_{2g} electron systems is not straightforwardly visible from the crystal structure alone because

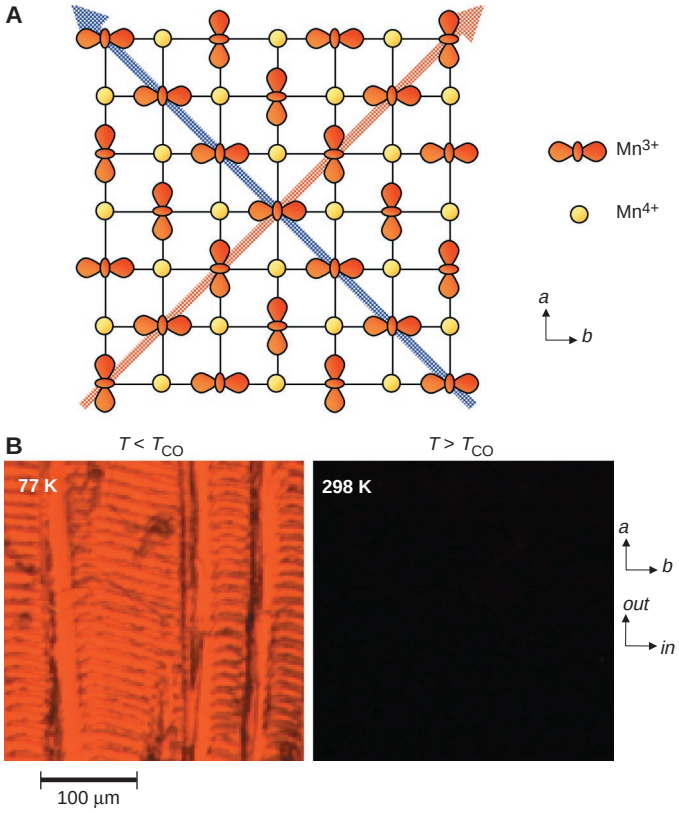

Fig. 3. (**A**) The orbital $[(3x^2 - r^2)/(3y^2 - r^2)]$ and charge order of the CE type projected on the MnO_2 sheet (*ab* plane). (**B**) Polarization microscope image with cross-polarization of incident and reflected light parallel to *a* and *b* axes for a $La_{0.5}Sr_{1.5}MnO_4$ ($x = 0.5$) crystal. The left bright image is for the charge/orbital–ordered state at 77 K. The orbital-disordered state at 298 K shows the isotropic optical response and hence gives the dark image.

of the relatively weak JT distortion of the t_{2g} electron. This is in contrast to the case of an e_g electron with strong JT distortion, but it provides a more challenging problem. In this context, the resonant x-ray scattering method recently developed by Murakami and coworkers (*27*) is a very powerful tool for probing these orbital-ordering patterns.

An example of dynamical orbital correlation is seen in the spin-state transition in $LaCoO_3$ with $3d^6$ configuration of Co. Around 100 K, the nonmagnetic and insulating state in $LaCoO_3$ undergoes a gradual transition from the low-spin state t_{2g}^6 ($S = 0$) to the intermediate-spin state $t_{2g}^5 e_g^1$ ($S = 1$). [The high-spin state $t_{2g}^4 e_g^2$ ($S = 2$) is predicted to be located at a higher energy level than the intermediate-spin state (*54*), as the latter gains a larger d-p hybridization energy in crystal lattice.] The intermediate-spin Co ion with one e_g electron is a JT ion, whereas the low-spin state has no orbital degree of freedom. In fact, the correlated local lattice distortion clearly shows up in the infrared phonon spectra in accord with the spin-state crossover (*55*), although the average lattice structure appears to be undistorted from that of the ground state. This is another example of thermally induced dynamical JT effect due to short-range orbital order, in addition to the case of the CMR manganese oxides. However, $LaCoO_3$ undergoes the insulator-to-metal transition by warming above 500 K. As predicted by the LDA calculation (*54*), this phenomenon may be interpreted as the loss of the orbital (short-range) order.

We have discussed only these limited examples, but most of the bandwidth- and/or filling (doping)–control Mott transition in the transition-metal oxides are more or less affected by the orbital order-disorder transition. Therefore, the orbital correlation and the spin correlation are expected to most often play an important role in charge dynamics in the metallic state near the Mott transition, which is termed "anomalous metal."

Theoretically, it is a fascinating problem to look for exotic states realized only with the orbital degrees of freedom. Especially intense interests have been focused on the quantum liquid states of the spin and/or orbital. To approach this problem, many authors study the model Hamiltonian (Eq. 1) with the rotational symmetry, i.e., SU(2) symmetry, also in the orbital space, where $\vec{T}$ enters into the Hamiltonian in the form of $\vec{T}_i \cdot \vec{T}_j$ as

$$H = \sum_{\langle ij \rangle} (x + \vec{S}_i \cdot \vec{S}_j)(y + \vec{T}_i \cdot \vec{T}_j) \qquad (3)$$

where $\langle ij \rangle$ is the nearest neighbor pair. The point $x = y = 1/4$ is a special one where the symmetry is enhanced from $[SU(2)]_{spin} \times [SU(2)]_{orbital}$ to SU(4) (*56*). The former corresponds to the respective rotation in the spin and orbital space, and the latter also includes the rotations between the spin and orbital space. At this SU(4)-symmetric point, the quantum fluctuations of both the spin and orbital are enhanced and the "SU(4) singlet" is more stable in comparison with the usual "spin SU(2) singlet." Therefore, the orbital degrees of freedom help the realization of the resonating valence bond spin liquid, which has been looked for with great interest but has not yet been found in quantum magnets without orbital degeneracy (e.g., La_2CuO_4). The basic unit of the SU(4) singlet is the plaquette, which might be realized in $LiNiO_2$ (*56*). The 1D model of Eq. 3 has recently been extensively studied (*57*–*62*). It shows five phases, including (i) the dimerized state of both $\vec{S}_i \cdot \vec{S}_{i+1}$ and $\vec{T}_i \cdot \vec{T}_{i+1}$ with the gap for the excitation spectra and (ii) the gapless state governed by the SU(4) symmetry (*62*).

In real materials, there should be no rotational symmetry in the orbital pseudospin space, and this anisotropy is expected to stabilize the ordered state because the quantum fluctuation is suppressed by the Ising-type anisotropy. However, it is also possible that this anisotropy gives rise to another type of quantum fluctuations, as will be discussed below. With doubly degenerate e_g orbitals,

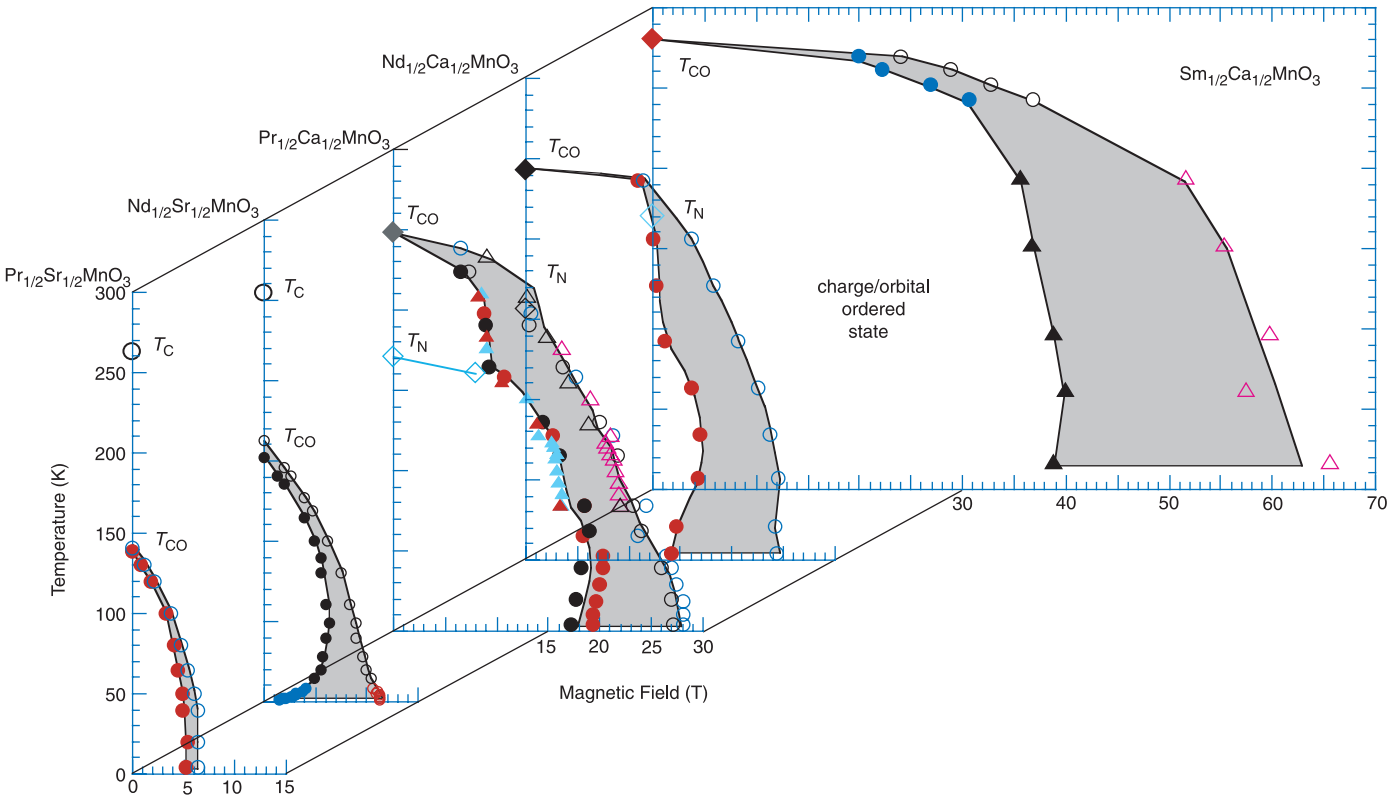

Fig. 4. The CE-type charge/orbital–ordering phase diagrams in the plane of magnetic field and temperature for various $R_{0.5}A_{0.5}MnO_3$ crystals, R and A being trivalent rare-earth and divalent alkaline-earth ions, respectively. T_C, T_N, and T_{CO} stand for the ferromagnetic, antiferromagnetic, and charge-ordering transition temperature, respectively.

the dominant part of the effective Hamiltonian for 3D perovskite structure is (*63*)

$$H_0 = \sum_i \sum_{\alpha = a,b,c} J\left[4(\vec{S}_i \cdot \vec{S}_{i+\alpha})\left(\tau_i^\alpha - \frac{1}{2}\right) \times \left(\tau_{i+\alpha}^\alpha - \frac{1}{2}\right) + \left(\tau_i^\alpha + \frac{1}{2}\right)\left(\tau_{i+\alpha}^\alpha + \frac{1}{2}\right)\right] \quad (4)$$

where $\tau_i^{a(b)} = (1/2)(-T_i^{3z} \pm \sqrt{3}T_i^x)$ and $\tau_i^c = T_i^z$. The classical ground state of H_0 is found to be highly degenerate; namely, an A-type 2D AF state with $(x^2 - y^2)$ orbital, a G-type 3D AF state with $(3z^2 - r^2)$ orbital, and two mixed-orbital phases are degenerate. Assuming that the fluctuation from the ordered state is small, the dispersion of the Gaussian orbital mode is 2D, which gives rise to the logarithmic divergence of the fluctuation. Therefore, it is possible that the ground state becomes quantum disordered when the quantum fluctuation is treated beyond the Gaussian approximation.

Another possibility is that the directional ordering of the orbital resolves the magnetic frustration by specifying the strong and weak bonds. In a triangular lattice (e.g., $LiVO_2$), it has been proposed that a pattern of orbital occupancy will lead to the isolated triangles whose spin ground state is the singlet (when each spin is $S = 1$) (*64*).

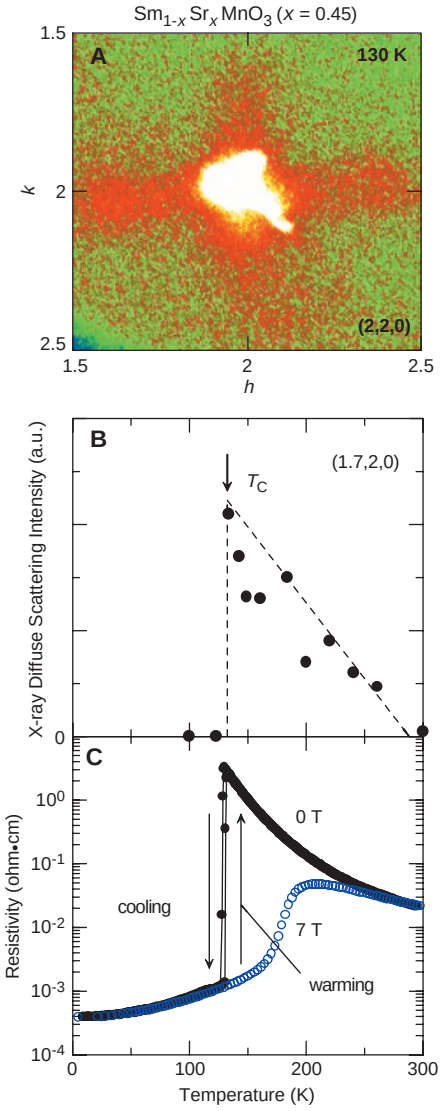

Fig. 5. (**A**) The diffused scattering feature around the (2, 2, 0) (in the orthorhombic setting) Bragg peak in the reciprocal space at 130 K, where the compound shows a typical CMR behavior. Temperature dependence of (**B**) x-ray diffuse scattering intensity (a.u., arbitrary units), reflecting the short-range charge-orbital correlations (JT polaron correlation) and (**C**) magnetotransport property for a $Sm_{1-x}Sr_x$ MnOI3 ($x = 0.45$) crystal on the verge of the charge/orbital–ordered state.

Conclusion

We have described some experimental and theoretical aspects of orbital physics in transition-metal oxides. The orbital degree of freedom is thought to play important roles, not only in the prominent case of the CMR manganese oxides but also in anisotropic electronic and magnetic properties of many transition-metal oxides. Taking the analogy to conventional materials phases, we may consider various states of orbital—not only solid (crystal) and liquid but even liquid crystal and glass. In fact, the short-range orbital order as seen in the CMR state (Fig. 5) may be viewed as the nematic-like liquid-crystal state of the orbital. Likewise, the orbital glass state may be realized in some frustrated or disordered lattice of transition-metal oxides, although the state has seldom been argued or unraveled experimentally. In this context, another attempt is the control of the orbital state in terms of external fields, not only with magnetic and stress fields as discussed above, but also through an electric field and light or x-rays. The electric field may directly affect the directional order of orbital, when the compound is insulating enough, and may alter the magnetic state. This is the orbital version of the liquid-crystal functionality. Additional visible effects by irradiation of light or x-rays have already been observed for the charge/orbital–ordered manganese oxide ($Pr_{1-x}Ca_xMnO_3$) as the light-induced melting of the charge/orbital order and resultant metallization (*65, 66*). Such an exotic and possibly ultrafast control of electronic and magnetic phases may find some applications in the future. Theoretically, the spin-charge-orbital coupled systems in transition-metal oxides offer the most fascinating and challenging arena to test many theoretical ideas, including quantum liquid, solid, and liquid-crystal states.

References and Notes

1. K. I. Kugel and D. I. Khomskii, *Sov. Phys. JETP* **52**, 501 (1981).
2. H. A. Kramers, *Physica* **1**, 182 (1934).
3. P. W. Anderson, in *Solid State Physics*, F. Seitz and D. Turnbull, Eds. (Academic Press, New York, 1963), vol. 14, p. 99.
4. J. Kanamori, *J. Phys. Chem. Solids* **10**, 87 (1959).
5. J. B. Goodenough, *Magnetism and Chemical Bond* (Interscience, New York, 1963).
6. H. A. Jahn and E. Teller, *Proc. R. Soc. London Ser. A* **161**, 220 (1937).
7. J. Kanamori, *J. Appl. Phys.* **31** (suppl.), 14S (1960).
8. G. A. Gehring and K. A. Gehring, *Rep. Prog. Phys.* **38**, 1 (1975).
9. C. Zener, *Phys. Rev.* **82**, 403 (1951).
10. P. W. Anderson and H. Hasegawa, *Phys. Rev.* **100**, 675 (1955).
11. For a review, see, for example, Y. Tokura, Ed., *Colossal Magnetoresistive Oxides* (Gordon and Breach Science, New York, 2000), and references therein.
12. For a review on theories of manganese oxides see, for example, an article by A. J. Millis in (*11*), pp. 53–86.
13. I. Solovyev, N. Hamada, K. Terakura, *Phys. Rev. Lett.* **76**, 4825 (1996).
14. T. Mizokawa and A. Fujimori, *Phys. Rev. B* **54**, 5368 (1996).
15. S. Ishihara, J. Inoue, S. Maekawa, *Phys. Rev. B* **55**, 8280 (1997).
16. H. Kuwahara, Y. Tomioka, A. Asamitsu, Y. Moritomo, Y. Tokura, *Science* **270**, 961 (1995).
17. H. Kawano *et al.*, *Phys. Rev. Lett.* **78**, 4253 (1997).
18. H. Kuwahara, T. Okuda, Y. Tomioka, A. Asamitsu, Y. Tokura, *Phys. Rev. Lett.* **82**, 4316 (1999).
19. R. Kajimoto *et al.*, *Phys. Rev. B* **60**, 9506 (1999).
20. R. Maezono, S. Ishihara, N. Nagaosa, *Phys. Rev. B* **58**, 11583 (1998).
21. Y. Konishi *et al.*, *J. Phys. Soc. Jpn.* **68**, 3790 (1999).
22. M. v. Zimmermann *et al.*, *Phys. Rev. Lett.* **83**, 4872 (1999).
23. J. B. Goodenough, *Phys. Rev.* **100**, 564 (1955).
24. V. I. Anisimov, I. S. Elfimov, M. A. Korotin, K. Terakura, *Phys. Rev. B* **55**, 15494 (1997).
25. I. Solovyev and K. Terakura, *Phys. Rev. Lett.* **83**, 2825 (1999).
26. J. Brink, G. Khaliullin, D. Khomskii, *Phys. Rev. Lett.* **83**, 5118 (1999).
27. Y. Murakami *et al.*, *Phys. Rev. Lett.* **80**, 1932 (1998).
28. T. Ishikawa, K. Ookura, Y. Tokura, *Phys. Rev. B* **59**, 8367 (1999).
29. F. Damay, C. Martin, A. Maignan, B. Raveau, *J. Appl. Phys.* **82**, 6181 (1997).
30. Y. Tokura, H. Kuwahara, Y. Moritomo, Y. Tomioka, A. Asamitsu, *Phys. Rev. Lett.* **76**, 3184 (1996).
31. L. Vasiliu-Doloc *et al.*, *Phys. Rev. Lett.* **83**, 4393 (1999).
32. S. Shimomura, N. Wakabayashi, H. Kuwahara, Y. Tokura, *Phys. Rev. Lett.* **83**, 4389 (1999).
33. K. Yamamoto, T. Kimura, T. Ishikawa, T. Katsufuji, Y. Tokura, *J. Phys. Soc. Jpn.* **68**, 2538 (1999).
34. Y. Tomioka *et al.*, *Appl. Phys. Lett.* **70**, 3609 (1997).
35. E. Saitoh, Y. Tomioka, T. Kimura, Y. Tokura, unpublished data.
36. D. S. Dessau *et al.*, *Phys. Rev. Lett.* **81**, 192 (1998).
37. Y. Okimoto *et al.*, *Phys. Rev. Lett.* **75**, 109 (1995).
38. D. D. Sarma *et al.*, *Phys. Rev. B* **53**, 6873 (1996).
39. T. Okuda *et al.*, *Phys. Rev. Lett.* **81**, 3203 (1998).
40. B. F. Woodfield, M. L. Wilson, J. M. Byers, *Phys. Rev. Lett.* **78**, 3201 (1997).
41. S. Ishihara, M. Yamanaka, N. Nagaosa, *Phys. Rev. B* **56**, 686 (1997).
42. F. Mack and P. Horsch, *Phys. Rev. Lett.* **82**, 3160 (1999).
43. Y. Motome and M. Imada, *Phys. Rev. B* **60**, 7921 (1999).
44. H. Shiba, R. Shiina, A. Takahashi, *J. Phys. Soc. Jpn.* **66**, 941 (1997).
45. A. Moreo, S. Yunoki, E. Dagotto, *Science* **283**, 2034 (1999).
46. L. P. Gorkov and V. Z. Kresin, *J. Supercond.* **12**, 243 (1999).
47. E. L. Nagaev, *Phys. Rev. B* **58**, 2415 (1998).
48. C. Castellani, C. R. Natoli, J. Ranninger, *Phys. Rev. B* **18**, 4945 (1978).
49. T. M. Rice, in *Spectroscopy of Mott Insulators and Correlated Materials*, A. Fujimori and Y. Tokura, Eds. (Springer, Berlin, 1995), pp. 221–229.
50. W. Bao, *Phys. Rev. Lett.* **78**, 507 (1997).
51. S. Yu. Ezhov, V. I. Anisimov, D. I. Khomskii, G. A. Sawatzky, *Phys. Rev. Lett.* **83**, 4136 (1999).
52. H. Sawada and K. Terakura, *Phys. Rev. B* **58**, 6831 (1998).
53. Y. Ren *et al.*, *Nature* **396**, 441 (1998).
54. M. A. Korotin *et al.*, *Phys. Rev. B* **54**, 5309 (1996).
55. S. Yamaguchi, Y. Okimoto, Y. Tokura, *Phys. Rev. B* **54**, R8666 (1997).

56. Y. Q. Li, M. Ma, D. N. Shi, F. C. Zhang, *Phys. Rev. Lett.* **81**, 3527 (1998).
57. A. A. Nersesyan and A. M. Tsvelik, *Phys. Rev. Lett.* **78**, 3939 (1997).
58. A. K. Kolezhuk and H.-J. Mikeska, *Phys. Rev. Lett.* **80**, 2709 (1998).
59. Y. Yamashita, N. Shibata, K. Ueda, *Phys. Rev. B* **58**, 9114 (1998).
60. B. Frischmuth, F. Mila, M. Troyer, *Phys. Rev. Lett.* **82**, 835 (1999).
61. P. Azaria, A. O. Gogolin, P. Lecheminant, A. A. Nersesyan, *Phys. Rev. Lett.* **83**, 624 (1999).
62. C. Itoi, S. Qin, I. Affleck, E-print available at xxx.lanl.gov/abs/cond-mat/9910109.
63. L. F. Feiner, A. M. Oles, J. Zaanen, *Phys. Rev. Lett.* **78**, 2799 (1997).
64. H. F. Pen, J. van den Brink, D. I. Khomskii, G. A. Sawatzky, *Phys. Rev. Lett.* **78**, 1323 (1997).
65. M. Fiebig, K. Miyano, Y. Tomioka, Y. Tokura, *Science* **280**, 1925 (1998).
66. V. Kiryukhin *et al.*, *Nature* **386**, 813 (1997).
67. The authors thank T. Fujiwara, M. Izumi, S. Ishihara, M. Kawasaki, G. Khaliullin, D. Khomskii, S. Maekawa, R. Maezono, Y. Murakami, Y. Okimoto, T. Okuda, E. Saitoh, K. Terakura, H. Yoshizawa, J. Zaanen, and F. C. Zhang for valuable discussions and collaborations. This work was supported by the Center of Excellence and Priority Areas Grants from the Ministry of Education, Science, and Culture of Japan and by the New Energy and Industrial Technology Development Organization.

REVIEW

Advances in the Physics of High-Temperature Superconductivity

J. Orenstein[1] and A. J. Millis[2]

The high-temperature copper oxide superconductors are of fundamental and enduring interest. They not only manifest superconducting transition temperatures inconceivable 15 years ago, but also exhibit many other properties apparently incompatible with conventional metal physics. The materials expand our notions of what is possible, and compel us to develop new experimental techniques and theoretical concepts. This article provides a perspective on recent developments and their implications for our understanding of interacting electrons in metals.

In a paper published in *Science* very shortly after the 1986 discovery of high–critical temperature (T_c) superconductivity by Bednorz and Müller, Anderson identified three essential features of the new superconductors (*1*). First, the materials are quasi–two-dimensional (2D); the key structural unit is the CuO_2 plane (Fig. 1), and the interplane coupling is very weak. Second, high-T_c superconductivity is created by doping (adding charge carriers to) a "Mott" insulator. Third, and most crucially, Anderson proposed that the combination of proximity to a Mott insulating phase and low dimensionality would cause the doped material to exhibit fundamentally new behavior, not explicable in terms of conventional metal physics.

In the ensuing years this prediction of new physics was confirmed, often in surprising ways. The challenge has become to characterize the new phenomena and to develop the concepts required to understand them. The past 5 years have been particularly exciting. Advances in crystal chemistry and in experimental techniques have created a wealth of information with remarkable implications for high-T_c and related materials. Here we focus on four areas where progress has been especially rapid: spin and charge inhomogeneities ("stripes"); the low-temperature properties of the superconducting state; phase coherence and the origin of the pseudogap; and the Fermi surface and its anisotropies in the nonsuperconducting or normal state.

Mott Insulators, Superconductivity, and Stripes

High-T_c superconductivity is found in copper oxide–based compounds with a variety of crystal structures, an example of which is shown in Fig. 1A. The key element shared by all such structures is the CuO_2 plane, depicted with an occupancy of one electron per unit cell in Fig. 1B. At this electron concentration the plane is a "Mott insulator," the parent state from which high-T_c superconductors are derived. A Mott insulator is a material in which the conductivity vanishes as temperature tends to zero, even though band theory would predict it to be metallic. Many examples are known, including NiO, $LaTiO_3$, and V_2O_3. [For recent reviews, see (*2, 3*).] However, the high-T_c cuprates are the only Mott insulators known to become superconducting when the electron concentration is changed from one per cell.

A Mott insulator is fundamentally different from a conventional (band) insulator. In the latter system, conductivity is blocked by the Pauli exclusion principle. When the highest occupied band contains two electrons per unit cell, electrons cannot move because all orbitals are filled. In a Mott insulator, charge conduction is blocked instead by electron-electron repulsion. When the highest occupied band contains one electron per unit cell, electron motion requires creation of a doubly occupied site. If the electron-electron repulsion is strong enough, this motion is blocked. The amount of charge per cell becomes fixed, leaving only the electron spin on each site to fluctuate. Doping restores electrical conductivity by creating sites to which electrons can jump without incurring a cost in Coulomb repulsion energy.

Virtual charge fluctuations in a Mott insulator generate a "super-exchange" (*4*) interaction, which favors antiparallel alignment of neighboring spins. In many materials, this leads to long-range antiferromagnetic order, as shown in Fig. 1. Anderson proposed that the quantum fluctuations of a 2D spin ½ system like the parent compound La_2CuO_4 might be sufficient to destroy long-range spin order. The resulting "spin liquid" would contain electron pairs whose spins are locked in an antiparallel or "singlet" configuration. The motion of such singlet pairs is akin to the resonance of π bonds in benzene, thus the term "resonating valence bond" (RVB). Anderson pointed out that the valence bonds resemble the Cooper pairs of Bardeen-Cooper-Schrieffer (BCS) superconductivity. A compelling picture of a Mott insulator as a suppressed version of the BCS state emerged: electrons dressed up in pairs, but with no place to go. Because the Mott insulator is naturally paired, Anderson argued, it would become superconducting if the average occupancy is lowered from one.

Soon after the discovery of high-T_c superconductivity, experiments revealed that the spin liquid state is not realized in the undoped cuprates. [It now seems likely that a spin liquid ground state exists for spin ½ particles on geometrically frustrated 2D lattices such as the Kagome (*5*).] Instead, the spins order in a commensurate antiferromagnetic pattern at a rather high Néel temperature between 250 and 400 K, depending on the material. The extent of the antiferromagnetic phase in the temperature versus carrier concentration plane of the high-T_c phase diagram is illustrated in Fig. 2. The Néel temperature drops very rapidly as the average occupancy is reduced from 1 to $1 - x$, reaching zero at a critical doping x_c of only 0.02 in the

[1]Department of Physics, University of California, Berkeley, CA 94720, USA, and Materials Science Division, Lawrence Berkeley National Laboratory, Berkeley, CA 94720, USA. [2]Department of Physics and Astronomy, Rutgers University, Piscataway, NJ 08854, USA.